Tribology International 185 (2023) 108524

Contents lists available at ScienceDirect

Tribology International

journal homepage: www.elsevier.com/locate/triboint

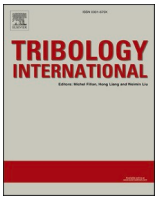

Utilising *H/E* to predict fretting wear performance of DLC coating systems

Samuel J. McMaster [a,*,1], Shahriar Kosarieh [a,2], Tomasz W. Liskiewicz [b], Anne Neville [a], Ben D. Beake [c]

[a] School of Mechanical Engineering, University of Leeds, Leeds LS2 9JT, UK
[b] Faculty of Science and Engineering, Manchester Metropolitan University, John Dalton Building, Chester Street, Manchester M15 6BH, UK
[c] Micro Materials Ltd., Willow House, Yale Business Village, Ellice Way, Wrexham LL13 7YL, UK

ARTICLE INFO

Keywords:
Fretting
DLC
Wear
Friction

ABSTRACT

Diamond-like carbon coatings have previously been studied as a protective coating for fretting wear protection providing low friction and low wear. *H/E* ratio has been used as a metric to rank coating performance in sliding wear, but this has not been applied to gross-slip fretting. Three DLC coating systems (a-C:H, Si-a-C:H, a-C:H:W top layers) on hardened M2 tool steel were studied using a bespoke electrodynamic shaker with a 10 mm 52100 steel ball as the counterface. This work has shown that H/E ratio can be used to predict wear performance in gross-slip fretting; the highest *H/E* ratio a-C:H performed best with low friction and wear.

1. Introduction

Fretting wear is small amplitude oscillatory wear between two surfaces in contact, generally under vibration [1,2]. The relation between *H/E* ratio and frictional performance is well understood across length scales in full sliding reciprocating wear tests and pin-on-disk [3–6] tests however little research has been performed to assess this relation in the fretting regime, specifically in the gross slip fretting regime where it is a step below reciprocating sliding with the additional contribution of surface fatigue. Gross-slip fretting is generally typified by damage mechanisms such as abrasive wear, oxidative wear and delamination [7–9]. Liskiewicz et al. [10] found that, for hard PVD coatings, a low Young's modulus (correlating with higher *H/E*) promoted low wear. High Young's modulus and an easily deformed substrate led to brittle cracking and accelerated wear due to the generation of wear debris in this work.

H/E can relate to frictional performance by taking into account the interfacial/adhesive component and ploughing component [11]. The ploughing component is responsible for the deformation of materials in the direction of sliding. As ploughing is expected to be smaller for sinking in than piling up, therefore the ploughing contribution to friction is expected to decrease with increasing *H/E* [6]. H^3/E^2 can also be used to relate tribological performance by considering contact yield pressure and fracture toughness from Hertzian contact analysis [3,12].

Diamond-like carbon (DLC) is a family of metastable amorphous carbon coatings, their properties vary depending upon their sp^2/sp^3 ratio, level of hydrogenation and any doping elements [13–17]. These coatings are typically characterised by high hardness, chemical inertness, and low coefficients of friction [16,18]. Blanpain et al. [19] conducted a study of the fretting wear performance of hard carbon coatings and found that the low coefficient of friction and wear rate of the coatings could be attributed to the formation of a lubricating third body. Kalin and Vižintin [20] conducted a lubricated fretting study on DLCs, they noted a wear rate and coefficient of friction multiple times lower than in uncoated contacts due to the reduction of adhesive wear and debris transfer. Dalibon et al. [21] noted good fretting behaviour for DLC coatings on nitrided martensitic stainless steel for low loads and short tests. Adhesion issues were present in longer tests. Navaneethakrishnan et al. [22,23] conducted multiple fretting studies on hydrogenated DLC on Ti-6Al-4V and found low friction and wear compared to uncoated samples; this was attributed to graphitisation and formation of a transfer layer on the alumina counterface.

In this study, an electro-dynamic shaker fretting tester was used to assess the fretting performance of three multi-layered DLC coatings at high contact pressures in dry conditions. The multi-layers were applied to improve the adhesion of the coatings to the substrate and to

Abbreviations: COF, Coefficient of friction; DLC, Diamond-like carbon; PACVD, Plasma-assisted chemical vapour deposition; PVD, Physical vapour deposition.

* Corresponding author.
E-mail address: ad6423@coventry.ac.uk (S.J. McMaster).
[1] Present address: Functional Materials and Chemistry Research Group, Coventry University, Priory Street, Coventry, CV1 5FB
[2] Present address: GKN Automotive GKN Driveline International GmbH, Hauptstr. 130, 53797 Lohmar, Germany

https://doi.org/10.1016/j.triboint.2023.108524
Received 29 January 2023; Received in revised form 5 April 2023; Accepted 15 April 2023
Available online 17 April 2023
0301-679X/© 2023 The Author(s). Published by Elsevier Ltd. This is an open access article under the CC BY license (http://creativecommons.org/licenses/by/4.0/).

compensate for DLC's high intrinsic residual stress [16,24,25]. Fouvry et al. [26] found that the introduction of compressive residual stresses can protect against cracking in a fretting contact. Du et al. [27] found that adhesion and coating toughness had a greater effect on fretting wear and fretting fatigue resistance than the friction reduction of DLCs and graphitic-like carbon coatings on a Ti-6AL-4V substrate. The dopants were added to obtain differences in the coating mechanical properties, which was performed previously by Tillmann et al. [28] and Beake and co-authors [29,30]. The hardened tool steel substrate was chosen as it was previously shown to provide load support [31] and can be used to model bearing steels where fretting is common [16,32,33].

The aim of this work was to analyse the mechanical properties of doped and undoped DLC coatings and assess whether it is possible to predict gross slip fretting friction and wear performance using the mechanical properties and the common wear ratios of H/E and H^3/E^2.

2. Methodology and Materials

2.1. Substrates and Coating Structures

Hardened M2 tool steel (HTS) was selected as the substrate for the DLC coatings due to its mechanical properties and ability to be heat treated [34]. Substrate coupons were initially cut from cylindrical steel bars (diameter = 25 mm) to a standardised thickness of 6 mm per coupon. A circular grinder with varying grades of silicon carbide polishing paper was used for polishing under water lubrication. Sequentially finer grit sizes (120, 300, 450, 600, 800 and 1200) were used to remove the machining marks and achieve the correct surface finish.

To obtain the optimal surface roughness (R_a = 0.01 μm target roughness), samples are further polished with sequential fibre polishing cloths (VerduTex and MicroFloc) and polycrystalline diamond suspension (9 μm and 3 μm VerduTex and 0.25 μm with MicroFloc). This resulted in a mirror-finished surface.

All coatings were deposited with the Hauzer Flexicoat 850 physical vapour deposition (PVD), and plasma-assisted chemical vapour deposition (PACVD) located in the School of Mechanical Engineering at the University of Leeds. The coatings will be referred by the following designations:

- a-C:H – Coating A
- Si-a-C:H – Coating B
- a-C:H:W – Coating C

The coating structures consist of Cr adhesive layers, WC gradient layers and the top DLC layer. The following deposition steps were used to produce the coatings [31]:

i. Chamber heating
ii. Target cleaning
iii. Plasma surface etching
iv. Cr layer deposition
v. Cr/WC deposition
vi. a-C:H:W deposition (final step for Coating C)
vii. a-C:H/Si-a-C:H deposition (for Coatings A and B respectively)

During the initial coating step, the chamber is pumped to 4×10^{-5} mbar and heated to 200 °C. Heating is engaged again during the plasma surface etching step; otherwise, the temperature is not controlled during the deposition. The pump was maintained at low power to vent waste gases from the chamber. Acetylene (C_2H_2) was used as the precursor gas for the top DLC layer in the PACVD process. Hexamethyldisiloxane (HMDSO), vaporised in the chamber, was used as the dopant for Coating B. A WC magnetron sputtering target was engaged to provide the doping for Coating C. These coatings are the same as those studied by McMaster et al. [31], further details of the deposition are present in this paper.

2.2. Coating Structures and Mechanical Properties

Coating thickness was studied by calotest with a 30 mm diameter ball [35–37] and confirmed with FIB-SEM (FEI Helios G4 CX Dualbeam SEM). Fig. 1 shows the cross-section layer structures of all three coatings. The adhesive (Cr) layer was 0.29 ± 0.03 μm for all coatings. The gradient (WC) layer was 0.89 ± 0.08 μm for all coatings. Pt was deposited to protect the coating surface during the focused-ion beam procedure.

Mechanical properties were determined by load-controlled partial load nanoindentation using a NanoTest Vantage system (Micro Materials, UK) with a Berkovich diamond indenter [31]. This results in a depth-sensitive measurement of mechanical properties however surface extrapolations have been used for this study. The plateau value was used for hardness and extrapolation to the surface was used for elastic modulus [38]. A total of 10 indentations with 40 loading points, in a range of 0–500 mN, per sample, was used. The indenter contact velocity was set to 0.50 μms^{-1}. The load and unload time for each indentation step was 2 s. A 1 s dwell was used at the maximum load to ensure there was no creep. A 60 s dwell period in the final unload step was used for thermal drift correction. The area function of the indenter was found by indentation into a fused silica reference sample. Hardness (H) and elastic modulus (E) were calculated by applying Oliver-Pharr analysis [39]. E and ν (0.2) are Young's modulus and Poisson's ratio for the coating; E_i (1140 GPa) and ν_i (0.07) are the same quantities for diamond respectively [40].

The roughness of all samples was measured using a topography scan using the NanoTest platform. A 4.5 μm radius spheroconical probe was used with a 200 μm scan distance and a probe velocity of 10 μms^{-1}. The load applied during this topographic scan was 0.1 mN. A total of 5 scans were performed across the surface of one sample. Each scan was performed with separation distance of 500 μm from the previous scan.

2.3. Fretting testing

Fretting tests were performed with a bespoke electrodynamic shaker driven fretting rig as shown in [41]. The system is controlled with a bespoke LabVIEW program. Tangential force during testing is monitored with a load cell. The optical displacement sensor adjusts the displacement of the electrodynamic shaker via a feedback loop to maintain it within the parameters specified. All fretting tests were performed in laboratory conditions with a temperature of 22 °C and a humidity of 34%.

The counterfaces for the testing were 10 mm diameter 52100 steel balls, this material was chosen as it is a common bearing steel [42–44]. Testing was performed in dry conditions with 15,000 wear cycles at a frequency of 5 Hz. This results in a test time of 50 min. The amplitude was set to ± 50 μm giving wear in the gross slip fretting regime (as determined using sliding ratio [45]). Sliding ratio is defined as the ratio between the displacement amplitude at zero Q and the maximum displacement amplitude ($\frac{\delta_0}{\delta}$) [45]. The effective velocity was 250 μms^{-1}. Three tests were performed to assess variability in the fretting friction. Tests were performed at a load of 20 N.

Table 1 summarises the sliding ratios and contact pressures in each of the test conditions as calculated by Hertzian contact mechanics [46–48]. These values were calculated to ensure that the gross-slip regime would be attained. The sliding ratio of the uncoated substrate was predicted to be 0.58. The Poisson's ratios for the 52100 steel, HTS and DLC were 0.285 [32], 0.285 [34] and 0.2 [16] respectively. The elastic moduli for the DLC and HTS can be found in Table 2. The elastic modulus used for 52100 steel was 200 GPa [42].

2.4. Microscopy and Wear Volume Analysis

Wear scars were imaged with a Leica DM6000M light microscope.

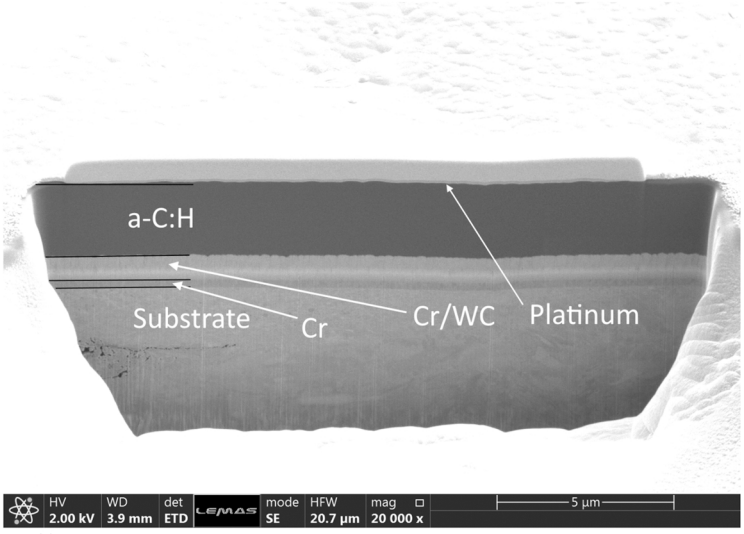

(a)

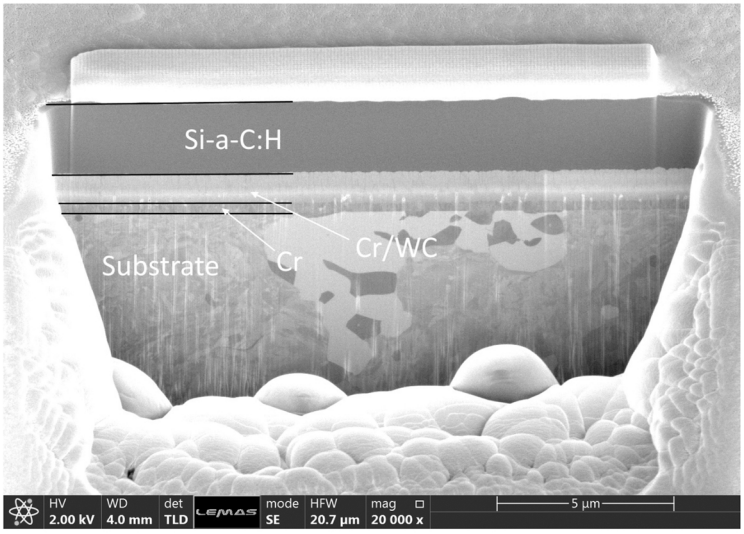

(b)

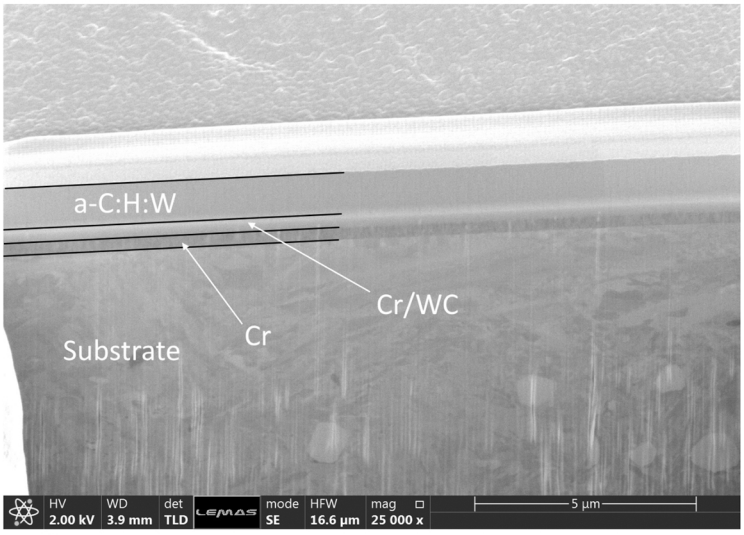

(c)

Fig. 1. FIB-SEM cross-sections of (a) Coatings A, (b) Coating B (b) and (c) Coating C. Micrographs of the same coating systems were studied in [31].

Table 1
Predicted contact pressures and sliding ratio conditions for fretting testing.

Coating	Predicted P_{max} (GPa)	Predicted Sliding Ratio
A	1.20	0.56
B	1.12	0.54
C	1.24	0.57

Wear volumes were analysed using a Bruker Alicona (Institute for Advanced Manufacturing and Engineering, Coventry University) using the 50x lens. These scans were further analysed using MountainsMap software to generate the wear volume data.

3. Results

3.1. Mechanical Properties

Coating and substrate mechanical properties and coating surface roughness is shown in Table 2. Surface mechanical properties of the coatings are determined by extrapolating multi-cycle (load-partial unload) nanoindentation to the surface (zero contact depth). Hardness (H) is found by taking the plateau value from the series of measurements as the initial indents will be lower than the true hardness [38], these values are less than 1/10 relative indentation depth as per ISO14577–4 [49]. The elastic modulus (E) is determined by taking the mean of the maximum range (extrapolating to the surface) to negate surface contact effects reducing the modulus at low contact depths [38]. For these coatings, using this method, the standard deviation for hardness and elastic modulus are ~0.7 GPa and ~5 GPa respectively. The same method was employed previously in the impact and erosion studies on these coating systems [31].

The HTS substrate shows distinct differences in its mechanical properties having a surface hardness of 10.0 GPa compared to the minimum hardness of 13.1 GPa for Coating B. The mean elastic modulus of HTS is higher than all coatings with a value of 239 GPa. This results in HTS having lower values of both H/E and H^3/E^2 (0.042 and 0.017 GPa respectively) compared to the coatings. The hardness of HTS is similar to that seen by Wilbur et al. [50] though a nitriding processing was used compared to the flame hardening for this study. Coating A had the highest hardness of the coatings (20.2 GPa). The highest mean elastic modulus for the coatings was on Coating C with a value of 218 GPa.

Despite the target surface preparation, the substrate was rougher than the nominal roughness with a value of 26 nm R_a compared to 10 nm R_a. Coatings A and C have the same mean surface roughness as the substrate however Coating B has a roughness value 12 nm R_a higher.

3.2. Fretting testing

3.2.1. Fretting logs and sliding ratio

By plotting the tangential force (Q) against the number of cycles and displacement, logs of the fretting process are obtained which can be used to visualise the fretting regime the system is in and whether this changes throughout the test. These logs were constructed in MATLAB. The tangential force data was processed through the de-trend function (in MATLAB) as the LabVIEW program compares the difference in the maxima and minima in tangential force per cycle to calculate friction resulting in some load cell drift throughout the test. Fig. 2 illustrates the fretting logs for different sample configurations. Each of the logs is in the gross slip fretting regime. With the addition of the DLC coating, the tangential force decreases resulting in lower energy dissipation [51,52]. Some variability is seen at the start of each test as the rig requires a few cycles to adjust to the specified parameters.

Fig. 3 shows how the sliding ratio changes throughout the test for uncoated HTS and Coating A. When the sliding ratio is below or equal to 0.26, the contact is in the partial slip regime; above 0.26, the contact is in the gross slip regime [41,45]. As the value remains above 0.26 through the entirety of the test, fretting in the gross slip regime is maintained throughout the test [45]. The relative stability of each test configuration can be assessed by analysing how smooth the sliding ratio progression is. The substrate is more unstable corresponding to the variability of its respective fretting map, this may be due to the generation of wear debris. However, the PID (proportional-integral-derivative) loop used to adjust the displacement for the fretting rig may play a part. A force is applied to displace the counterface and the displacement measured by an optical sensor. This displacement is then continually adjusted by calculating the proportional, integral, and derivative responses to meet the target displacement. The proportional term incorporates proportional changes for error (difference between the

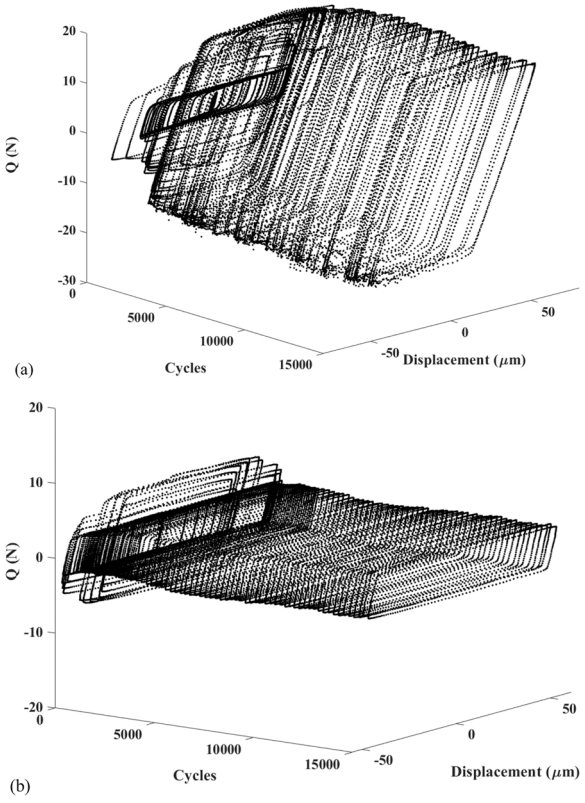

Fig. 2. Fretting logs for uncoated HTS and Coating A. (a) Uncoated HTS. (b) Coating A.

Table 2
Average mechanical properties for the substrates and coating structures.

Substrate /DLC recipe	DLC Coating Thickness (μm)	Surface Roughness (nm R_a)	Surface hardness, H (GPa)	Mean Elastic Modulus, E (GPa)	H/E	H^3/E^2 (GPa)
HTS	N/A	26 ± 4	10.0 ± 0.3	239 ± 7	0.042 ± 0.002	0.017 ± 0.001
A	2.20 ± 0.20	26.0 ± 10.3	20.2	199	0.101	0.207
B	2.17 ± 0.16	48.0 ± 12.4	13.1	164	0.080	0.083
C	1.17 ± 0.12	26.2 ± 1.9	13.9	218	0.064	0.056

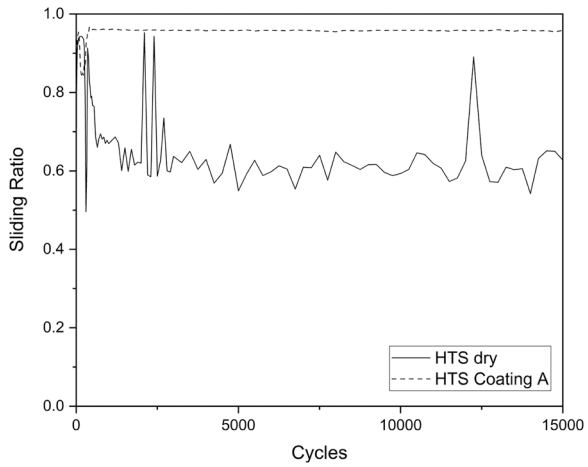

Fig. 3. Sliding ratio variation with cycles for uncoated substrate, and Coating A.

desired value and process variable). The integral term examines the process variable over time and correct the output by reducing the offset from the process variable. The derivative part of the control system monitors the rate of change of the process variable and changes the output when there are unusual variations [53]. The higher tangential force measured on the uncoated substrate as seen in Fig. 2 may cause the system to attempt to adjust to a greater degree but it cannot fully compensate for the variations throughout the test. The coated systems have a lower tangential force (requiring a lower level of error correction) and therefore the sliding distance was closer to the nominal displacement. For the coated samples, the sliding ratio was stable throughout the test. The sliding ratio was monitored continuously the test to ensure that all systems remained within the gross-slip regime.

3.2.2. Coefficient of Friction

In gross slip fretting it is common to have some instability in the friction, especially during the early parts of a test where friction is high. Generally, it will then reduce to a lower steady state value [54]. Discontinuity or change in COF signifies that there are severe metal/-substrate interactions [55]. This can indicate that there is wear through or decohesion of the coating.

Fig. 4 shows the fretting friction results of the coating variants at 20 N. The COF is averaged over each cycle (both positive and negative displacement) and the error bars are a result of averaging the repeated tests at the specific number of cycles indicated in the figure. This allows for the deviation at each stage of the test to be analysed. Tests on the uncoated substrate showed a high COF of approximately 0.9 however this is not present in the figure as the primary samples for analysis were the coatings. This friction level is typical of unlubricated steel-on-steel contact [56]. Coating A had a steady state COF of 0.15. Coating B had a slightly lower COF, but its running period is much more pronounced. Coating C had a less pronounced running in period but towards the end of the cycles, the friction begins to climb.

To further investigate the running in behaviour, Fig. 5(a) shows the first 1000 cycles of the fretting tests. Coating A achieved stable friction by approximately 500 cycles, but Coating B had a COF that climbs up to 600 cycles with a value of 0.35. Coating C begins with low friction but this climbs to 0.24 at 300 cycles before steadily increasing after 5000 cycles. This increases later in the test as demonstrated in Fig. 4. Fig. 5(b) shows the individual fretting friction plots for Coating B. These individual friction traces, it can be seen that the large uncertainty in this coating system was due to variability in the length of the running in period, being significantly longer in the first test where the COF only fell after approximately 7000 cycles.

Fig. 6 summarises the coefficients of friction of tested configurations. The COF was averaged over all the cycles. Therefore, those with large errors represent tests in which there was a large period of instability such as Coating B. Though Coating C's COF rises it had a less severe running in period thereby giving a smaller error bar. The lowest COF is achieved with Coating A with a value of 0.17.

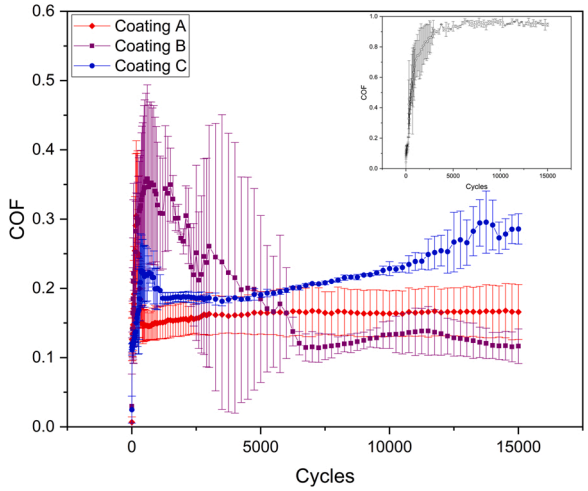

Fig. 4. COF evolution of Coatings A, B and C. Inset shows the COF evolution of the uncoated substrate.

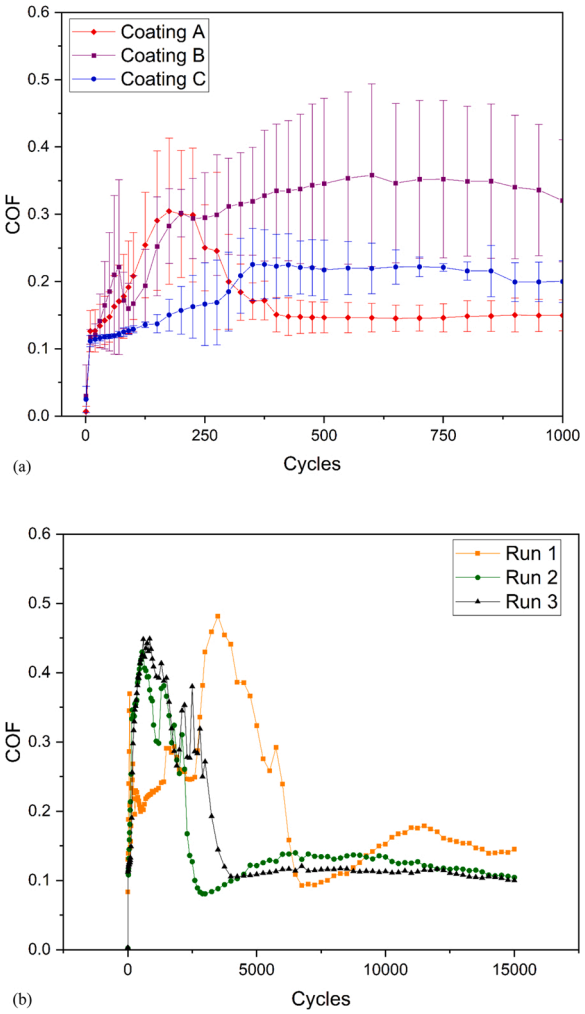

Fig. 5. Fretting friction plots of (a) the first 1000 cycles Coatings A, B and C and (b) the individual plots for Coating B.

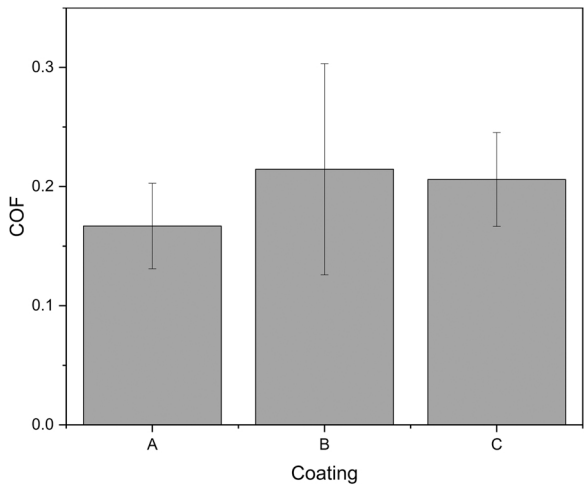

Fig. 6. Average COF of all the coating configurations.

3.2.3. Dissipated energy

By integrating the frictional force and displacement of each loop and cumulatively summing the energies, the total dissipated fretting energy can be calculated. This can be used as a metric to compare the resistance to wear of each system [55]. In general, for a simplified interface with uncoated materials, lower dissipated energy results in reduced fretting wear. However, in multi-layered materials, the interactions between different layers and their varying wear rates can result in the breakdown of this simple relationship. As total dissipated energy is a product of the displacement and tangential force, this would also correlate to a lower coefficient of friction averaged over the entire fretting cycle. By comparing this quantitative metric with the wear morphology of each fretting scar a more complete picture of the system performance can be obtained.

Fig. 7 shows the total dissipated energy of all three coatings systems. Coating C had the highest total dissipated energy with a value of 12 J. Coating A had a lower variance in the dissipated energy due to its stable friction, but Coating B had a slightly lower total dissipated energy. The uncoated substrate had a dramatically higher total dissipated energy of 30 J under the same conditions.

3.2.4. Wear Morphology

Optical microscopy was used to image the fretting wear scars to qualitatively assess their morphology. Fig. 8 shows the morphology of the fretting scars of the coatings and the uncoated substrate. Coating A displays abrasive marks in the centre of the wear scar with some ejected wear debris. This is similar for Coating B however the volume of ejected wear debris is greater in the case of B. Coating C displays a far larger volume of wear debris and the coating is worn through in the middle of the wear scar. The contrast differences in the centre of the wear scar provides evidence of this wear through. Uncoated HTS had the largest wear in this set of fretting scars. There is evidence of large, oxidised wear debris being ejected from the fretting surface alongside an oxidised contact circle.

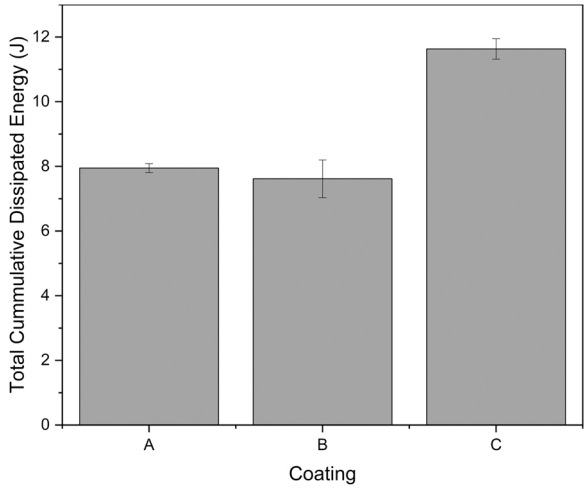

Fig. 7. Cumulative dissipated energy of Coatings A, B and C.

3.3. Wear Volume

Fig. 9 shows the comparison between the wear volume (as determined using the Bruker Alicona) and the cumulative dissipated energy as derived from the fretting logs. This approach was used previously by Fouvry and co-authors [10,55,57]. There is a weak positive correlation between the wear volume and cumulative dissipated energy; Coatings A and B had similar levels of dissipated energy (as shown in Fig. 7), but Coating B had a much larger wear volume.

Fig. 10 shows a plot of H/E vs wear volume where there is a strong negative correlation. Coating A (with the highest H/E) had the lowest measured wear volume.

H^3/E^2, as a measure of the load carrying capacity of a coating system, also correlates with wear volume. H^3/E^2 correlates with H/E as explored by Beake [29]. Fig. 11 shows the plot of H^3/E^2 against wear volume. The correlation is stronger for this parameter compared to H/E with Pearson's r and R^2 values of approximately 0.99.

Fig. 12(a) shows an example of the wear scar (uncoated HTS) as imaged by the Bruker Alicona and processed by MountainsMap software. Coating B in Fig. 12(b) had a lower smaller fretting wear scar in both diameter and depth. The increased surface roughness of this sample is visible in this scan. Ring lighting was used as it illuminates the surface evenly and ensures optimal measurement conditions [58].

4. Discussion

Friction coefficient is generally not directly measured as often as wear in fretting tests. Wear is a far more present issue due to its severity by crack nucleation and propagation (under cyclic fatigue conditions) and eventual formation of wear debris [59]. Friction does however play a part in determining the regime of fretting currently being experienced alongside the displacement relative to the contact area [8,9,45,57]. An energy-based approach is often favourable as this can quantify the fretting lifetime and resultant wear depth [57]. Fig. 9 shows the relation between wear volume and dissipated energy. With respect to the error of using 3D optical microscopy to measure wear, Ayerdi et al. [60] explored different wear volume determination methods and found that compared to the ASTM G133–05 and ASTM D7755–11 standards and cross section profile integration over length, 3D topographical methods produced a maximum error of 3.3%. Although cumulative dissipated energy has been used as a proxy for wear volume it may not always be entirely suitable as noted by the low R^2 value (≈0.40) in Fig. 9. A certain amount of energy input is required to initiate wear and therefore it may take some time before wear is measurable, this results in the minimum energy shown in the figure being approximately 6 J. Surface roughness and dynamic surface modification effects may also introduce further complications.

The application of coatings to protect against fretting damage has been long understood. Coatings that have residual compressive stresses can be particularly useful as they protect against cracking phenomena [26]. Liskiewicz et al. [10,61] analysed the durability of a series of hard coatings under fretting wear establishing the total dissipated energy density allowable to the coating system before failure occurs. The mechanical properties of these coatings were noted to affect their durability with a high Young's Modulus producing the highest wear (on TiN). The difference in modulus between the substrate and coating negatively

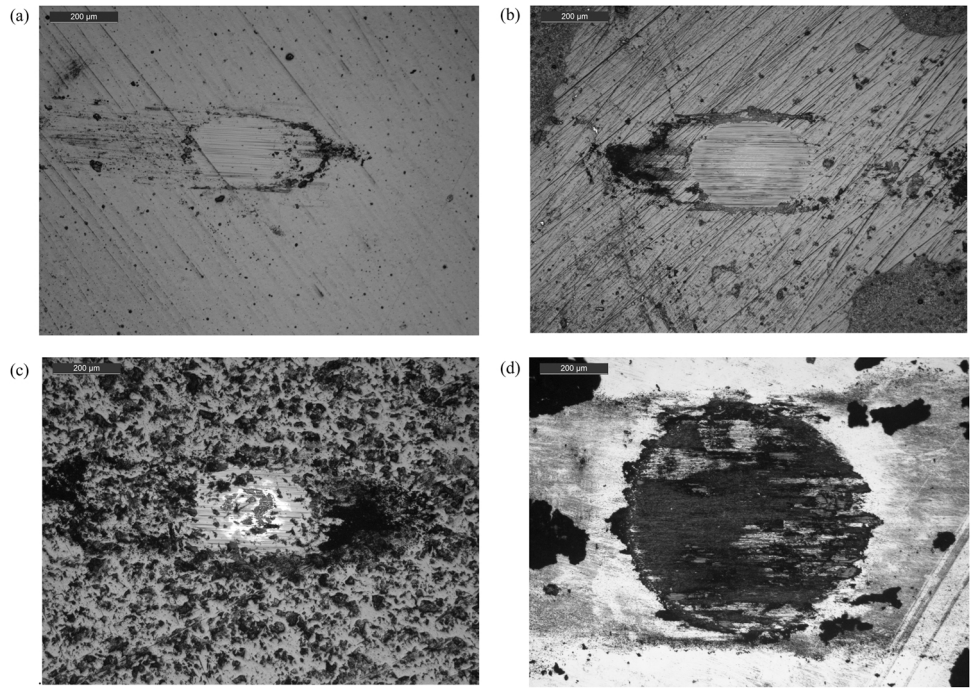

Fig. 8. Morphology of fretting wear scars on HTS. (a) Coating A. (b) Coating B. (c) Coating C. (d) Uncoated HTS.

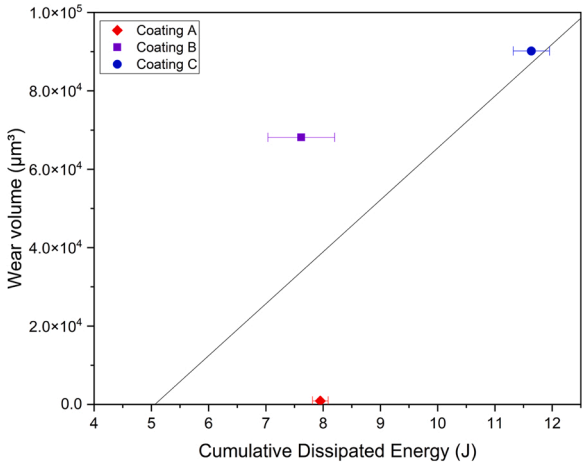

Fig. 9. A plot of wear volume vs cumulative dissipated energy for Coatings A, B and C. Pearson's r = 0.63512. R^2 = 0.40337.

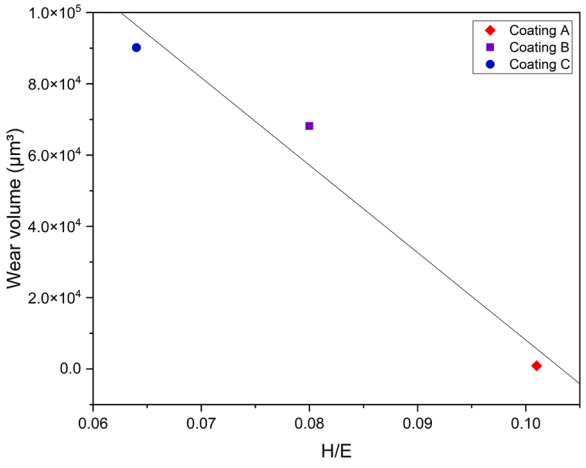

Fig. 10. Relation between H/E and wear volume for Coatings A, B and C. Pearson's r = −0.978721. R^2 = 0.91576.

affected wear performance, leading to easier deformation of the substrate and brittle cracking generating wear particles. Comparing the modulus differences in Table 2, this is less of a concern with these coatings however the tests were not run until total coating structure failure. This could be the topic of further study with longer testing times.

In an approach where a coating is being chosen to protect a surface, a reduction in the friction coefficient results in lower tangential forces (when visualised as part of a fretting loop/map) and therefore reduces the dissipated energy over a number of fretting cycles [62]. This should reduce the amount of wear and increase coating lifetime. Therefore, an investigation into the relationship between mechanical properties and their prediction of frictional and wear performance is beneficial for future coating optimisation in fretting wear scenarios.

Considering both the surface roughness and thickness (Table 2) and analysing the friction in Fig. 4, Fig. 5 and Fig. 6, we can see that Coating A (with the highest H/E ratio) performs best. The wear volume in Fig. 8 is extremely low. The relation between wear volume and H/E in Fig. 10 and wear volume and H^3/E^2 in Fig. 11 further supports the superior performance of Coating A. The early friction instability in Coating B in Fig. 5(a) results in a higher variance in the COF in Fig. 6, but the dissipated energy is similar between Coating A and B. The high surface roughness of Coating B (≈48 nm R_a compared to ≈26 nm R_a for Coatings A and C) likely influenced this frictional instability. This is can be observed in the breakdown of the different test runs in Fig. 5(b). Coating C had approximately 1 µm less of the top layer coating (Table 2) and this is likely the reason for the rise in COF after 5000 cycles (Fig. 4); the wearing through of the top layer could generate wear debris which will increase the friction. Alternatively, the removal of the top layer of the coating could result in the metal counterface rubbing against the metal interlayer thereby causing an increase in friction and wear [56]. Liskiewicz et al. [63] studied a similar set of DLC coatings using nano-indentation and nano-fretting. The nano-fretting utilised a 5 µm radius sphero-conical probe to produce initial contact pressures in the range of 11–15 GPa. Despite the difference in length scale, Coating A also had

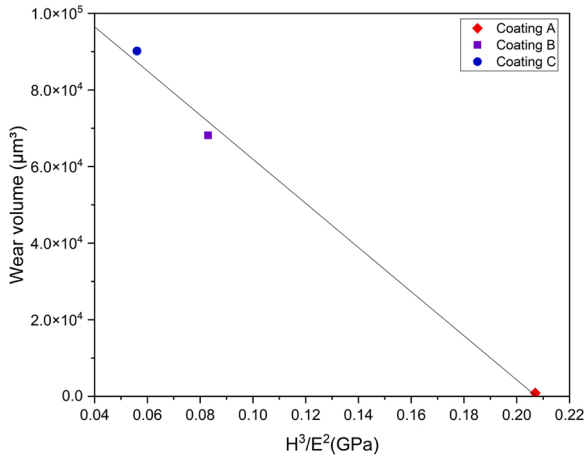

Fig. 11. Relation between H^3/E^2 and wear volume for Coatings A, B and C. Pearson's r = −0.99751. R^2 = 0.99503.

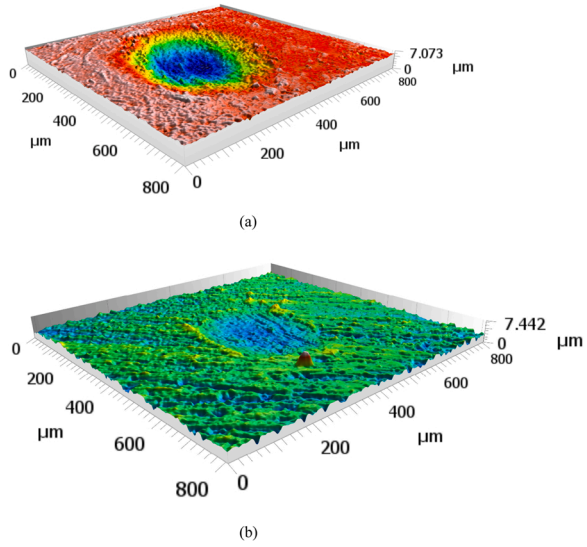

Fig. 12. Surface profile scan of fretting wear scars by confocal microscopy. (a) Uncoated HTS. (b) Coating B.

a smaller wear volume and friction force. Coating C was also thinner as in this work, but the wear was still within the top layer coating. The plot between H/E against wear volume as shown in Fig. 10 indicates that the mechanical properties can be neatly used to predict gross-slip fretting performance. H^3/E^2 also correlates (shown in Fig. 11 with Peason's r and R^2 values of ≈0.99) however the mathematical operation of generating this metric exaggerates the numerical values as shown in Table 2[3,4,29]. Beake [29] states that calibration accuracy is more important for H^3/E^2 as error in E will cause a larger error in H^3/E^2. Additionally, within set of similar coatings, differences in H^3/E^2 are larger than H/E [29]. Complex relationships have previous been demonstrated with similar DLC coating systems by Bai et al. [64]. In this study, non-doped Si-doped and W-doped were studied under reciprocating dry sliding conditions at frequencies of 1 Hz, 6 Hz and 36 Hz. Oxidative wear dominated on Si-doped DLC (like Coating B) which degraded performance at higher sliding velocities. Lanigan et al. [65] produced a tri-doped DLC (Si,O,F) that had enhanced wear resistance compared to Si-DLC. This coating appeared to produce a SiOF species in the wear track that limited oxidative wear.

The high friction coefficient (0.9) observed for the uncoated substrate as evidenced by the large fretting log in Fig. 2, is typical of the friction values of uncoated metals under fretting conditions. A COF of 0.8 was recorded for AISI1034 and Ti-6Al-4 V alloys with a 52100 steel ball (with a diameter of 25.4 mm) [56].

Fretting tests were performed previously on W-doped DLC (Balinit C Star, Oerlikon Balzers) on Ti-6Al-4V and SCMV steel by Mohd Tobi et al. [66], though at a lower contact pressure (due to the larger contact area). No delamination of the coating was observed and a COF of 0.3 was seen for the DLC layer. This is within the range seen in Fig. 4, though the frictional increases were seen due to layer wear through over part of the fretting scar. The average friction is lower in Fig. 6 however due to the running in dynamics noted in Fig. 5(a). This increase in friction towards the end of the test was also seen with Balinit C Star coated on Ti-6Al-4V [66]. Backscatter electron microscopy with EDX confirmed the wear through to the CrN interlayer in this case but the substrate remained coated. Blanpain et al. [19] compared the fretting wear of a series of carbon coatings and found that the COF was between 0.05 and 0.10 (with a 10 mm diameter corundum ball) depending on the deposition methodology employed to create the DLC (either radio frequency (RF), arc or laser). Additionally, the wear rate was found to be smaller compared to TiN. The low friction was supposed to be due to the formation of a graphitised transfer layer. The formation of wear debris in Fig. 8, indicates that a lubricating third body could be present but further study would be required to provide evidence of graphitisation [67–73].

5. Conclusion

In this study, fretting testing was performed utilising an electrodynamic shaker to assess the relation between coating H/E ratio and the gross-slip fretting wear performance. Dissipated energy and H/E ratio were assessed as a proxy for wear volume measurements.

Under dry conditions, the coatings perform according to their H/E ratio with Coating A (highest H/E) displaying the lowest COF and wear volume. Coating C was partially worn through though it was approximately 1 µm thinner which will contribute to the wear performance. No load support effects were seen in changing the substrate unlike in impact wear studies on these same coating structures [31]. Though Coating B had a similar cumulative dissipated energy compared to Coating A, it had a larger COF with greater variance during the testing cycles resulting in higher wear. In conclusion, H/E (and also H^3/E^2) can be used to indicate gross-slip fretting wear performance of multi-layer DLC coating systems under unlubricated conditions.

It would be beneficial in future work to analyse the tribofilm [74–78] formed and assess its dynamics over the testing time. In-situ tribofilm formation studies or performing multiple tests at different numbers of cycles would be ideal for this purpose. A greater number of cycles could also be employed to properly investigate the wear through of the coatings and evaluate the global energy input required to cause failure as employed previously by Liskiewicz and Fouvry [55]. Post-test Raman spectroscopy could be used to identify the level of graphitisation experienced by the coatings (measurable change in the I_D/I_G ratio within the wear scar) [71] and this could be correlated with nanoindentation mapping of the fretting scars [79] to track the dynamic change the coating structure with wear (measurable softening of the coating due to the change of structure).

CRediT authorship contribution statement

Samuel J. McMaster: Methodology, Validation, Investigation, Resources, Writing – original draft, Visualization. **Shahriar Kosarieh:** Methodology, Validation, Writing – review & editing, Supervision. **Tomasz W. Liskiewicz:** Conceptualization, Methodology, Resources, Writing – review & editing, Supervision, Funding acquisition. **Anne Neville:** Conceptualization, Supervision, Funding acquisition. **Ben D. Beake:** Conceptualization, Resources, Writing – review & editing, Supervision, Funding acquisition.

Declaration of Competing Interest

The authors declare the following financial interests/personal relationships which may be considered as potential competing interests; Samuel J. McMaster reports travel was provided by Jost Foundation.

Data Availability

Data will be made available on request.

Acknowledgements

This work was supported by the Engineering and Physical Sciences Research Council (EPSRC), Grant No. ELP01629X and Micro Materials Ltd. as part of the EPSRC Doctoral Training Centre in Integrated Tribology (iT-CDT). The authors would like to thank Ishmaeel Ghouri, Mihhail Stotsjuk and Lei Cao for running some of the fretting tests. Rizwan Tai and Ranveer Matharu of Coventry University are thanked for collecting the Alicona wear volume scans and for processing the data. The Jost Foundation is thanked for its financial support in awarding a travel grant to attend ISFF10 in Leuven, Belgium.

Statement of Originality

The authors state that the work presented in this article is original. The article has not been submitted to any journal prior to this submission and the article is not in consideration for publication in any other journal.

References

[1] Waterhouse RB. Fretting wear. Wear 1984;100:107–18. https://doi.org/10.1016/0043-1648(84)90008-5.
[2] Waterhouse RB. Fretting fatigue. Mater Sci Eng 1976;25:201–6. https://doi.org/10.1016/0025-5416(76)90071-9.
[3] Chen X, Du Y, Chung YW. Commentary on using H/E and H3/E2 as proxies for fracture toughness of hard coatings. Thin Solid Films 2019. https://doi.org/10.1016/j.tsf.2019.04.040.
[4] Leyland A, Matthews A. On the significance of the H/E ratio in wear control: a nanocomposite coating approach to optimised tribological behaviour. Wear 2000;246:1–11. https://doi.org/10.1016/S0043-1648(00)00488-9.
[5] Cheng YT, Cheng CM. Scaling, dimensional analysis, and indentation measurements. Mater Sci Eng R: Rep 2004;44:91–149. https://doi.org/10.1016/j.mser.2004.05.001.
[6] Ni W, Cheng YT, Lukitsch MJ, Weiner AM, Lev LC, Grummon DS. Effects of the ratio of hardness to Young's modulus on the friction and wear behavior of bilayer coatings. Appl Phys Lett 2004;85:4028–30. https://doi.org/10.1063/1.1811377.
[7] Zhu MH, Zhou ZR. On the mechanisms of various fretting wear modes. Tribol Int, vol. 44. Elsevier; 2011. p. 1378–88. https://doi.org/10.1016/j.triboint.2011.02.010.
[8] Vingsbo O, Söderberg S. On fretting maps. Wear 1988;126:131–47. https://doi.org/10.1016/0043-1648(88)90134-2.
[9] Zhou ZR, Nakazawa K, Zhu MH, Maruyama N, Kapsa Ph, Vincent L. Progress in fretting maps. Tribol Int 2006;39:1068–73. https://doi.org/10.1016/j.triboint.2006.02.001.
[10] Liskiewicz T, Fouvry S, Wendler B. Hard coatings durability under fretting wear. Tribology and Interface Engineering Series, vol. 48. Elsevier,; 2005. p. 657–65. https://doi.org/10.1016/S0167-8922(05)80067-7.
[11] Beake BD, Harris AJ, Liskiewicz TW. Review of recent progress in nanoscratch testing. Tribology - Mater, Surf Interfaces 2013;7:87–96. https://doi.org/10.1179/1751584X13Y.0000000037.
[12] Johnson KL. Contact mechanics. Cambridge University Press; 1985.
[13] Robertson J. Diamond-like amorphous carbon. Mater Sci Eng: R: Rep 2002;37:129–281. https://doi.org/10.1016/S0927-796X(02)00005-0.
[14] Pierson HO. Handbook of Carbon, Graphite, Diamonds and Fullerenes: Processing, Properties and Applications (Materials Science and Process Technology). Noyes Publications; 1993. https://doi.org/10.1016/B978-0-8155-1339-1.50008-6.
[15] Grill A. Diamond-like carbon: state of the art. Diam Relat Mater 1999;8:428–34. https://doi.org/10.1016/S0925-9635(98)00262-3.
[16] Hainsworth S v, Uhure NJ. Diamond like carbon coatings for tribology: production techniques, characterisation methods and applications. Int Mater Rev 2007;52:153–74. https://doi.org/10.1179/174328007X160272.
[17] Lifshitz Y. Diamond-like carbon — present status. Diam Relat Mater 1999;8:1659–76. https://doi.org/10.1016/S0925-9635(99)00087-4.
[18] Grill A. Review of the tribology of diamond-like carbon. Wear 1993;168:143–53. https://doi.org/10.1016/0043-1648(93)90210-D.
[19] Blanpain B, Celis JP, Roos JR, Ebberink J, Smeets J. A comparative study of the fretting wear of hard carbon coatings. Thin Solid Films 1993;223:65–71. https://doi.org/10.1016/0040-6090(93)90728-8.
[20] Kalin M, Vižintin J. The tribological performance of DLC coatings under oil-lubricated fretting conditions. Tribol Int 2006;39:1060–7. https://doi.org/10.1016/j.triboint.2006.02.040.
[21] Dalibon EL, Pecina JN, Cabo A, Trava-Airoldi VJ, Brühl SP. Fretting wear resistance of DLC hard coatings deposited on nitrided martensitic stainless steel. J Mater Res Technol 2018. https://doi.org/10.1016/j.jmrt.2017.12.004.
[22] Navaneethakrishnan P, Ganesh Sundara Raman S, Gnanamoorthy R, Ravi N. Relative performance of hydrogenated, argon-incorporated and nitrogen-incorporated diamond-like carbon coated Ti-6Al-4V samples under fretting wear loading. Thin Solid Films 2009;517:4365–71. https://doi.org/10.1016/j.tsf.2009.03.061.
[23] Navaneethakrishnan P, Ganesh Sundara Raman S, Pathak SD, Gnanamoorthy R, Ravi N. Fretting wear studies on diamond-like carbon coated Ti-6Al-4V. Surf Coat Technol 2009;203:1205–12. https://doi.org/10.1016/j.surfcoat.2008.10.017.
[24] Pauleau Y. Residual stresses in DLC films and adhesion to various substrates. Tribology of Diamond-Like Carbon Films: Fundamentals and Applications. Boston, MA: Springer US; 2008. p. 102–36. https://doi.org/10.1007/978-0-387-49891-1_4.
[25] Lin Y, Zia AW, Zhou Z, Shum PW, Li KY. Development of diamond-like carbon (DLC) coatings with alternate soft and hard multilayer architecture for enhancing wear performance at high contact stress. Surf Coat Technol 2017;320:7–12. https://doi.org/10.1016/j.surfcoat.2017.03.007.
[26] Fouvry S, Fridrici V, Langlade C, Kapsa Ph, Vincent L. Palliatives in fretting: a dynamical approach. Tribol Int 2006;39:1005–15. https://doi.org/10.1016/j.triboint.2006.02.038.
[27] Du D, Liu D, Ye Z, Zhang X, Li F, Zhou Z, et al. Fretting wear and fretting fatigue behaviors of diamond-like carbon and graphite-like carbon films deposited on Ti-6Al-4V alloy. Appl Surf Sci 2014;313:462–9. https://doi.org/10.1016/j.apsusc.2014.06.006.
[28] Tillmann W, Lopes Dias NF, Stangier D, Matveev S, Thomann CA, Debus J. Structure and tribo-mechanical properties of Si- and W-containing amorphous carbon based multilayers. Appl Surf Sci Adv 2021:5. https://doi.org/10.1016/j.apsadv.2021.100105.
[29] Beake BD. The influence of the H/E ratio on wear resistance of coating systems – Insights from small-scale testing. Surf Coat Technol 2022:128272. https://doi.org/10.1016/j.surfcoat.2022.128272.
[30] Beake BD, Liskiewicz TW, Vishnyakov VM, Davies MI. Development of DLC coating architectures for demanding functional surface applications through nano- and micro-mechanical testing. Surf Coat Technol 2015;284:334–43. https://doi.org/10.1016/j.surfcoat.2015.05.050.
[31] McMaster SJ, Liskiewicz TW, Beake BD, Neville A. Probing Fatigue Resistance in Multi-layer DLC Coatings by Micro-impact: Correlation to Erosion Tests. Surf Coat Technol 2020;402:126319. https://doi.org/10.1016/j.surfcoat.2020.126319.
[32] Voevodin AA. Hard DLC Growth and Inclusion in Nanostructured Wear-protective Coatings. Tribology of Diamond-Like Carbon Films. Boston, MA: Springer US,; 2008. p. 263–81. https://doi.org/10.1007/978-0-387-49891-1_9.
[33] Maruyama T, Saitoh T, Yokouchi A. Differences in mechanisms for fretting wear reduction between oil and grease lubrication. Tribology Trans 2017;60:497–505. https://doi.org/10.1080/10402004.2016.1180469.
[34] AZoM. M2 Molybdenum High Speed Tool Steel (UNS T11302). AZO Material 2012:3–5. https://www.azom.com/article.aspx?ArticleID=6174 (Accessed 27 July 2018).
[35] Mala Z, Vitu T, Novakova D. Determination of coating thickness - industrial standard in the physics practical education. Phys Teach Eng Educ 2011:4.
[36] Holmberg K (Kenneth), Matthews A (Allan). Coatings tribology: properties, mechanisms, techniques and applications in surface engineering. Elsevier Science,; 2009.
[37] Hernández LC, Ponce L, Fundora A, López E, Pérez E. Nanohardness and residual stress in TiN coatings. Materials 2010;4:929–40. https://doi.org/10.3390/ma4050929.
[38] Fischer-Cripps AC. Critical review of analysis and interpretation of nanoindentation test data. Surf Coat Technol 2006;200:4153–65. https://doi.org/10.1016/j.surfcoat.2005.03.018.
[39] Oliver WC, Pharr GM. An improved technique for determining hardness and elastic modulus using load and displacement sensing indentation experiments. J Mater Res 1992;7:1564–83. https://doi.org/10.1557/JMR.1992.1564.
[40] Pharr GM, Oliver WC. Measurement of thin film mechanical properties using nanoindentation. MRS Bull 1992;17:28–33. https://doi.org/10.1557/S0883769400041634.
[41] Wade A, Copley R, Alsheikh Omar A, Clarke B, Liskiewicz T, Bryant M. Novel numerical method for parameterising fretting contacts. Tribol Int 2020;149:105826. https://doi.org/10.1016/j.triboint.2019.06.019.
[42] AZoM. AISI 52100 Alloy Steel (UNS G52986). AZO Materials 2012:1–2. https://www.azom.com/article.aspx?ArticleID=6704 (accessed 27 July 2018).
[43] Siu JHW, Li LKY. An investigation of the effect of surface roughness and coating thickness on the friction and wear behaviour of a commercial MoS2-metal coating on AISI 400C steel. Wear 2000;237:283–7. https://doi.org/10.1016/S0043-1648(99)00349-X.
[44] Fouvry S, Kapsa P, Vincent L. Fretting behaviour of hard coatings under high normal load. Surf Coat Technol 1994;68–69:494–9. https://doi.org/10.1016/0257-8972(94)90207-0.

[45] Fouvry S, Kapsa Ph, Vincent L. Analysis of sliding behaviour for fretting loadings: determination of transition criteria. Wear 1995;185:35–46. https://doi.org/10.1016/0043-1648(94)06582-9.
[46] Williams J. Engineering tribology, vol. 9780521609. Cambridge: Cambridge University Press; 2005. https://doi.org/10.1017/CBO9780511805905.
[47] Arnell D. Mechanisms and laws of friction and wear. Tribology and Dynamics of Engine and Powertrain: Fundamentals, Applications and Future Trends. Elsevier Ltd,; 2010. p. 41–72. https://doi.org/10.1533/9781845699932.1.41.
[48] Fischer-Cripps AC. Contact Mechanics. Nanoindentation 2004:1–20. https://doi.org/10.1007/978-1-4757-5943-3_1.
[49] ISO. ISO 14577–4:2016 Metallic materials — Instrumented indentation test of hardness and materials parameters Part 1: Test method 2016:19.
[50] Wilbur PJ, Davis JA, Wei R, Vajo JJ, Williamson DL. High current density, low energy, ion implantation of AISI-M2 tool steel for tribological applications. Surf Coat Technol 1996;83:250–6. https://doi.org/10.1016/0257-8972(95)02830-7.
[51] Fouvry S, Kapsa P, Sauger E, Martin JM, Ponsonnet L, Vincent L. Tribologically transformed structure in fretting. Wear 2002;245:39–52. https://doi.org/10.1016/s0043-1648(00)00464-6.
[52] Fantetti A, Tamatam LR, Volvert M, Lawal I, Liu L, Salles L, et al. The impact of fretting wear on structural dynamics: experiment and simulation. Tribol Int 2019;138:111–24. https://doi.org/10.1016/j.triboint.2019.05.023.
[53] Borase RP, Maghade DK, Sondkar SY, Pawar SN. A review of PID control, tuning methods and applications. Int J Dyn Control 2021;9:818–27. https://doi.org/10.1007/s40435-020-00665-4.
[54] Hintikka J, Mäntylä A, Vaara J, Frondelius T, Lehtovaara A. Stable and unstable friction in fretting contacts. Tribol Int 2019;131:73–82. https://doi.org/10.1016/j.triboint.2018.10.014.
[55] Liskiewicz T, Fouvry S. Development of a friction energy capacity approach to predict the surface coating endurance under complex oscillating sliding conditions. Tribol Int 2005;38:69–79. https://doi.org/10.1016/j.triboint.2004.06.002.
[56] Kubiak KJ, Liskiewicz TW, Mathia TG. Surface morphology in engineering applications: Influence of roughness on sliding and wear in dry fretting. Tribol Int 2011;44:1427–32. https://doi.org/10.1016/j.triboint.2011.04.020.
[57] Fouvry S, Liskiewicz T, Kapsa Ph, Hannel S, Sauger E. An energy description of wear mechanisms and its applications to oscillating sliding contacts. Wear 2003;255:287–98. https://doi.org/10.1016/S0043-1648(03)00117-0.
[58] Grochalski K, Wieczorowski M, H'Roura J, Le Goic G. The optical aspect of errors in measurements of surface asperities using the optical profilometry method. Front Mech Eng 2020:6. https://doi.org/10.3389/fmech.2020.00012.
[59] Fouvry S, Kapsa P, Vincent L. Quantification of fretting damage. Wear 1996;200:186–205. https://doi.org/10.1016/S0043-1648(96)07306-1.
[60] Ayerdi JJ, Aginagalde A, Llavori I, Bonse J, Spaltmann D, Zabala A. Ball-on-flat linear reciprocating tests: Critical assessment of wear volume determination methods and suggested improvements for ASTM D7755 standard. Wear 2021:470–1. https://doi.org/10.1016/j.wear.2021.203620.
[61] Liskiewicz T. Hard coatings durability under fretting. wear 2005. https://doi.org/10.1016/S0167-8922(05)80067-7.
[62] Ma L, Eom K, Geringer J, Jun TS, Kim K. Literature review on fretting wear and contact mechanics of tribological coatings. Coatings 2019;9:1–20. https://doi.org/10.3390/coatings9080501.
[63] Liskiewicz TW, Beake BD, Schwarzer N, Davies MI. Short note on improved integration of mechanical testing in predictive wear models. Surf Coat Technol 2013;237:212–8. https://doi.org/10.1016/j.surfcoat.2013.07.044.
[64] Bai M, Yang L, Li J, Luo L, Sun S, Inkson B. Mechanical and tribological properties of Si and W doped diamond like carbon (DLC) under dry reciprocating sliding conditions. Wear 2021;484–485:204046. https://doi.org/10.1016/j.wear.2021.204046.
[65] Lanigan JL, Wang C, Morina A, Neville A. Repressing oxidative wear within Si doped DLCs. Tribol Int 2016;93:651–9. https://doi.org/10.1016/j.triboint.2014.11.004.
[66] Mohd Tobi AL, Shipway PH, Leen SB. Gross slip fretting wear performance of a layered thin W-DLC coating: Damage mechanisms and life modelling. Wear 2011;271:1572–84. https://doi.org/10.1016/j.wear.2010.12.073.
[67] Field SK, Jarratt M, Teer DG. Tribological properties of graphite-like and diamond-like carbon coatings. Tribol Int 2004;37:949–56. https://doi.org/10.1016/j.triboint.2004.07.012.
[68] Mahajan SS, Barshilia HC, Mehta BR, Vankar VD. On the determination of the sp3 to sp2 ratio in diamond-like carbon thin films. Thin Solid Films 1997;302:250–5. https://doi.org/10.1016/S0040-6090(96)09519-3.
[69] Kosarieh S, Morina A, Flemming J, Lainé E, Neville A. Wear mechanisms of hydrogenated DLC in oils containing MoDTC. Tribol Lett 2016:64. https://doi.org/10.1007/s11249-016-0737-0.
[70] Rodriguez BJ, Navabpour P, Proprentner D, Walker M, Sun H, Schiller TL. An alternative approach to the tribological analysis of Si-doped DLC coatings deposited with different bias voltages using Raman spectroscopy mapping. Emergent Mater 2021. https://doi.org/10.1007/s42247-021-00263-w.
[71] Haque T, Morina A, Neville A, Kapadia R, Arrowsmith S. Effect of oil additives on the durability of hydrogenated DLC coating under boundary lubrication conditions. Wear 2009;266:147–57. https://doi.org/10.1016/j.wear.2008.06.011.
[72] Ogwu AA, Lamberton RW, Morley S, Maguire P, McLaughlin J. Characterization of thermally annealed diamond like carbon (DLC) and silicon modified DLC films by Raman spectroscopy. Phys B Condens Matter 1999;269:335–44. https://doi.org/10.1016/S0921-4526(99)00138-6.
[73] Solis J, Zhao H, Wang C, Verduzco JA, Bueno AS, Neville A. Tribological performance of an H-DLC coating prepared by PECVD. Appl Surf Sci 2016;383:222–32. https://doi.org/10.1016/j.apsusc.2016.04.184.
[74] Tamulevičius S, Meškinis Š, Tamulevičius T, Rubahn HG. Diamond like carbon nanocomposites with embedded metallic nanoparticles. Rep Prog Phys 2018;81:024501. https://doi.org/10.1088/1361-6633/aa966f.
[75] Humphrey E, Morris NJ, Rahmani R, Rahnejat H. Multiscale boundary frictional performance of diamond like carbon coatings. Tribol Int 2020;149:105539. https://doi.org/10.1016/j.triboint.2018.12.039.
[76] Jiang J, Arnell RD. On the running-in behaviour of diamond-like carbon coatings under the ball-on-disk contact geometry. Wear 1998;217:190–9. https://doi.org/10.1016/S0043-1648(98)00178-1.
[77] Erdemir A, Donnet C. Tribology of diamond-like carbon films: recent progress and future prospects. J Phys D Appl Phys 2006;39:R311–27. https://doi.org/10.1088/0022-3727/39/18/R01.
[78] Podgornik B, Vižintin J, Jacobson S, Hogmark S. Tribological behaviour of WC/C coatings operating under different lubrication regimes. Surf Coat Technol 2004;177–178:558–65. https://doi.org/10.1016/S0257-8972(03)00927-7.
[79] Liskiewicz T, Kubiak K, Comyn T. Nano-indentation mapping of fretting-induced surface layers. Tribol Int 2017;108:186–93. https://doi.org/10.1016/j.triboint.2016.10.018.